Journal of Materials Science and Chemical Engineering, 2025, 13(9), 31-54
https://www.scirp.org/journal/msce
ISSN Online: 2327-6053
ISSN Print: 2327-6045

Characterization and Pozzolanic Reactivity of Two Togolese Clays for Use as Supplementary Cementitious Materials

Dilami Diana Babakoua[1,2], Koffi Fiaty[2], Catherine Charcosset[2], Sanonka Tchegueni[1*], Komla Mawoulikplim Anove[1], Moursalou Koriko[1], Gado Tchangbedji[1]

[1]Laboratoire de Gestion, Traitement et Valorisation des Déchets (GTVD), Faculté des Sciences, Université de Lomé, Lomé, Togo
[2]Laboratoire d'Automatique, de Génie des Procédés et de Génie Pharmaceutique (LAGEPP), UMR CNRS 5007, Université Claude Bernard Lyon 1, Villeurbanne, France
Email: *tchegsani@gmail.com

How to cite this paper: Babakoua, D.D., Fiaty, K., Charcosset, C., Tchegueni, S., Anove, K.M., Koriko, M. and Tchangbedji, G. (2025) Characterization and Pozzolanic Reactivity of Two Togolese Clays for Use as Supplementary Cementitious Materials. *Journal of Materials Science and Chemical Engineering*, **13**, 31-54.
https://doi.org/10.4236/msce.2025.139003

Received: July 24, 2025
Accepted: September 7, 2025
Published: September 10, 2025

Abstract

Calcined clays, emerging as one of the most promising supplementary cementitious materials (SCMs), have gained global attention as key contributors to low-carbon cement production. This study investigates the potential use of two clays from different regions of Togo as SCMs. The clays were calcined between 700˚C and 900˚C to evaluate the influence of calcination temperature on their physicochemical properties. Their characteristics were analysed through XRF, XRD, FTIR, and TGA analyses. In addition, their pozzolanic reactivity was assessed using the TGA-based R3 test to quantify their calcium hydroxide consumption. Results showed that one clay was rich in kaolinite and the other in quartz. XRD and FTIR analyses suggested that 700˚C was sufficient to induce optimal transformation in both clays, while TGA analysis indicated that the kaolinite-rich clay achieved better results at 750˚C. For the clay rich in quartz, the ideal calcination temperature remains unclear due to its complex thermal properties. However, the R3 test confirmed the effectiveness of both clays as SCMs, with the kaolinite-rich clay exhibiting significantly higher reactivity than the other clay.

Keywords

SCMs, Low-Carbon Cement, R3 Test, Kaolinite, Quartz

1. Introduction

The cement industry accounts for approximately 7% of global CO_2 emissions, mainly due to clinker production, a key component of Ordinary Portland Cement

(OPC) [1]. During clinker production, the calcination of limestone ($CaCO_3$) releases significant amounts of CO_2, making it a major issue for decarbonization efforts. To address these challenges, there is a growing focus on reducing the clinker factor in cement through its substitution with alternative materials called supplementary cementitious materials (SCMs). These materials have been shown to effectively contribute to reducing the carbon footprint of OPC, while improving its performance and durability.

Based on their chemical composition, SCMs can be classified into hydraulic and pozzolanic materials [2]. Among existing pozzolanic materials, calcined clays, particularly kaolinitic clays, have emerged as highly promising due to their global availability, low cost, and proven reactivity when properly activated. Their activation generally involves heating to temperatures up to 800˚C. During this process, the kaolinite in clays undergoes a transformation into metakaolinite, an amorphous phase that reacts with calcium hydroxide ($Ca(OH)_2$), a by-product of the cement hydration reaction. This reaction leads to the formation of additional cementitious phases, such as calcium silicate hydrates (C-S-H), which contribute to improving the mechanical properties and durability of cementitious systems [3]. This makes calcined clays an interesting option for reducing the reliance on clinker.

Despite this proven advantage of calcined clays, their application remains underexplored in some regions, including Togo, where the available clay resources are not yet fully exploited for this purpose. However, investigative efforts carried out in several other countries have demonstrated the significant potential of calcined clays as SCMs [4]. This advancement surrounding calcined clays is a collective international effort, with various countries contributing to different aspects of research and application. However, collaborative studies conducted by research groups of K. Scrivener in Switzerland and F. Martirena from Cuba have significantly driven global focus, particularly through the development of cement blends incorporating calcined clays and limestone known as Limestone Calcined Clays Cement (LC3) [4]-[7]. These blends have been shown to reduce the clinker content down to 50% while maintaining similar mechanical properties and enhancing durability [4]. Later joined by India, these three countries have been actively involved in research and pilot projects for the implementation of this technology [8]-[10]. Through ongoing efforts to expand it to other countries, Colombia became the first to establish permanent industrial production and commercialization [8] [11].

Besides that, other countries have also been focusing their research on the use of calcined clays for sustainable cement production. In Africa, countries such as Malawi, Kenya, South Africa, Nigeria, Ghana, Burkina Faso, and a few others have conducted relevant research on the use of locally available clay resources as SCMs, confirming their potential to contribute to the development of low-carbon cement and reduce the environmental impact of cement production [12]-[17]. Furthermore, some companies on the Ivory Coast and Cameroon have started commer-

cializing LC3 cements [11]. In Togo, the government has recently initiated the development of national standards for cement production, aiming to ensure cement quality and safety by regulating raw materials, manufacturing processes, and final product characteristics [18]. Although these standards do not mainly cover the use of calcined clays, they may promote their adoption in the future, with the ambition to eventually establish national standards for the production of LC3 cements. In support of such initiatives and global efforts to decarbonize the cement sector, investigating the potential use of Togolese clay resources as SCMs appears relevant. Moreover, as the effectiveness of clays as SCMs is highly dependent on their mineralogical composition, which can vary significantly based on their geological origin, assessing their mineralogical composition is crucial when considering their utilisation.

This study focuses on the characterisation and pozzolanic reactivity of two clays from Togo in order to evaluate their potential as SCMs. Advanced analytical techniques, including X-ray fluorescence (XRF), X-ray diffraction (XRD), Fourier transform infrared (FTIR) spectroscopy, and thermogravimetric analysis (TGA), were used to investigate their chemical, mineralogical, and thermal properties. These techniques are widely recognised for their effectiveness in assessing the suitability of clay resources for use as SCMs [19].

A previous study by Anove *et al.* [20] explored the characterisation and use of the same clays, calcined at 750˚C, for geopolymer synthesis. In the present work, the investigation was extended to a wider calcination temperature range (700˚C - 900˚C) to better understand their thermal activation process. Additionally, TGA results were further exploited to estimate the kaolinite content of the clays and to monitor their dehydroxylation process.

Most importantly, their pozzolanic reactivity was assessed using a TGA-based R3 test. Recent studies have, in fact, highlighted the relevance of the R3 test for evaluating the pozzolanic reactivity [21] [22]. This approach provides new insights into the suitability of these clays as SCMs. The outcomes of this study are expected to contribute to the growing body of knowledge on the use of locally sourced materials in sustainable construction. By identifying their optimal calcination conditions and evaluating their reactivity, this research aims to support the development of sustainable cementitious materials that can contribute to reducing the environmental impact of the cement industry.

2. Materials and Methods

2.1. Sampling and Pre-Processing

Two clay samples were obtained from a previous sampling conducted by Anove *et al.* [20] in distinct quarries located respectively at Afagnan (6˚29'39"N; 1˚37'56"E, southern Togo) and Bandjeli (9˚25'05"N; 0˚37'12"E, northern Togo). The samples were hermetically sealed and stored until their use in the present study.

The raw clays were subjected to grinding in a Rocklabs RM 1000 vibratory disc mill and were sieved to 63 µm using an AS400-Retsch sieve shaker to ensure com-

parable particle size for both samples. The sieved samples were then calcined for 2 h in alumina crucibles at the following temperatures: 700˚C, 750˚C, 800˚C, 850˚C, and 900˚C. These temperatures were chosen based on preliminary studies and literature review indicating the temperature range of kaolinite transformation into metakaolinite between 600˚C and 900˚C [23]-[25]. However, it has been shown that calcination temperatures slightly higher than 600˚C provide better reactivity [26]. Calcination was carried out under ambient atmospheric conditions with a 3 h heating ramp in an electric muffle furnace (LE 0611P300, Nabertherm). The final processed samples, both raw and calcined, were stored at room temperature in airtight polypropylene containers until analysis.

2.2. Characterisation Techniques

A series of instrumental techniques, including XRF, XRD, FTIR, and TGA, was used to characterise both raw and calcined clays.

2.2.1. X-Ray Fluorescence (XRF) Analysis

The chemical composition of the raw clay samples was determined by X-ray fluorescence (XRF).

Sample preparation: The initially stored clay samples were prepared as pressed pellets in aluminium cups. The clay powders were manually mixed with a wax binder (Licowax micropowder) in a ratio of 10/0.5. The mixture was then pressed at 25 tons into pellets using an xrPress MT25 hydraulic press. The binder was used to enhance the cohesion and mechanical stability of pellets, preventing cracking during high-pressure pressing and ensuring a smooth, homogeneous surface for analysis.

Measurement and data collection: The prepared pellets were analysed using a Bruker S6 JAGUAR XRF spectrometer, and the data were processed with SPECTRA ELEMENTS software.

2.2.2. X-Ray Diffraction (XRD) Analysis

XRD was employed to identify the crystalline phases present in the raw clays and to observe their transformations during calcination.

Sample preparation: As with XRF analysis, proper sample preparation is essential prior to conducting measurements. The initially stored clay samples were placed in poly(methyl methacrylate) sample holders and pressed with a polished glass slide to ensure a smooth and uniform surface.

Measurement and data collection: XRD measurements were conducted using a Bruker D8 Advance diffractometer in the Bragg-Brentano horizontal θ-θ geometry. The equipment was operated at 40 kV and 40 mA with a Cu Kα radiation source (λ = 1.5406 Å). X-ray diffractograms were collected over a 2θ range of 5˚to 70˚.

Qualitative phase identification: The obtained diffraction patterns were analysed with Malvern Panalytical HighScore Plus 5.2 software. Powder Diffraction Files (PDF-2) from the International Centre for Diffraction Data (ICDD) and the

Crystallographic Open Database (COD) were used to identify mineral phases.

2.2.3. Fourier Transform Infrared (FTIR) Spectroscopy

FTIR analysis was performed to identify the functional groups present in the clay samples and to assess the chemical changes induced by calcination.

Measurement and spectra acquisition: The samples were analysed using a Nicolet iS50 FTIR spectrometer (Thermo Fisher Scientific) fitted with an Attenuated Total Reflectance (ATR) module. For each measurement, the clay powders were placed directly on the surface of the instrument's ATR crystal and pressed against it with a pressure applicator. The IR spectra were recorded in absorbance mode over the mid-infrared region (4000 - 400 cm^{-1}). The measurements consisted of an accumulation of 32 scans with an optical resolution of 2 cm^{-1} in 2 min. The background corrections were made with an air spectrum.

Qualitative analysis: Spectra were processed and analysed using OMNIC Spectra 9 (Thermo Fisher Scientific) software.

2.2.4. Thermogravimetric Analysis (TGA)

TGA was used to study the thermal behaviour of the clays and to calculate their kaolinite content.

Sample measurement: The samples were analysed using a Netzsch TG 209 F1 Libra thermal analyser. Approximately 10 - 12 mg of sample were placed in alumina crucibles, chosen for their thermal stability and inertness. The samples were then heated in the apparatus from 30˚C to 1000˚C at a heating rate of 10˚C/min under a nitrogen atmosphere to prevent oxidation.

Data analysis: After measurement, the weight loss as a function of temperature was recorded. The data were then analysed with Netzsch Proteus Thermal Analysis software to identify the different temperature ranges at which significant weight loss occurred.

Quantitative analysis: The weight loss between 400˚C and 600˚C, associated with the dehydroxylation of kaolinite [27]-[29], was used to quantify the kaolinite content in both raw and calcined clays. This was done according to equations (1) and (2), using the tangent method, previously described by [30]. This method minimises the influence of other mineral phases by focusing on the dehydroxylation temperature range. To check the reproducibility, two repetitions were carried out for each sample to calculate the mean value and the standard deviation (SD). Calculations were performed using Excel 2019 software.

$$Wt\%_{kaolinite,\,raw} = Wt\%_{kaol-OH,\,raw} \times \frac{M_{kaolinite}}{2M_{water}} \tag{1}$$

$$Wt\%_{kaolinite,\,cal} = Wt\%_{kaol-OH,\,cal} \times \frac{M_{kaolinite}}{2M_{water}} \times \frac{\left(100 - Wt\%_{kaol-OH,\,cal}\right)}{100} \tag{2}$$

where

$Wt\%_{kaolinite,\,raw}$ refers to the weight of kaolinite (%) in the raw clays.

$Wt\%_{kaolinite,\,cal}$ refers to the weight of kaolinite (%) in the calcined clays, indi-

cating the portion of unreacted kaolinite during calcination.

$Wt\%_{kaol-OH}$ represents the weight loss due to kaolinite dehydroxylation.

$M_{kaolinite}$ (258.16 g·mol^{-1}) and M_{water} (18.02 g·mol^{-1}) are the molecular weights of kaolinite and water, respectively.

As explained by [29], for calcined clays, due to the evaporation of water during calcination, the total mass of calcined clays differs from that of the raw clays. Therefore, the amount of remaining kaolinite after calcination has to be adjusted based on the residual water content, as indicated in Equation (2).

The calcined kaolinite content ($Wt\%_{calcined\ kaolinite}$), representing the amount of reacted kaolinite during calcination, was then obtained according to Equation (3).

$$Wt\%_{calcined\ kaolinite} = Wt\%_{kaolinite,\ raw} - Wt\%_{kaolinite,\ cal} \tag{3}$$

Beyond kaolinite quantification, the thermogravimetric (TG) spectra of the raw clays were also used to determine their moisture content and loss on ignition (LOI).

2.3. Pozzolanic Reactivity Test (TGA-Based R3 Method)

The pozzolanic reactivity of the clays was evaluated using the TGA-based R3 method described by Sivakumar *et al.* [31], which relies on the quantification of calcium hydroxide ($Ca(OH)_2$) consumption through TGA analysis. No reference pozzolan, such as pure metakaolin, was tested for comparison.

Preparation of R3 pastes: The R3 pastes were prepared following the recommendations of the ASTM C1897-20 standard [32] by mixing 10 g of clay with 30 g of calcium hydroxide and 5 g of calcium carbonate ($CaCO_3$). The dried powders were homogenised manually and then mixed with 54 mL of a potassium solution (4 g KOH and 20 g K_2SO_4 in 1 L of deionised water), both preconditioned at 40˚C. The pastes were stirred at 1600 rpm for 2 min, sealed, and cured in an oven at 40˚C for 7 days.

Hydration stoppage: After the 7-day curing period, 3 g of the hydrated hardened pastes were crushed to between 1 and 3 mm using a mortar and pestle. The crushed sample was then immediately immersed in 50 mL of isopropanol for 15 min to stop the hydration process. The suspension was stirred for 2 min, then filtered under vacuum using a fritted funnel. The retained solid was then collected, dried at 40˚C for 8 min, and stored in a desiccator until analysis.

$Ca(OH)_2$ consumption: $Ca(OH)_2$ consumption was quantified by TGA analysis, performed under a nitrogen atmosphere at a heating rate of 10˚C/min from 30˚C to 950˚C. The mass loss between 400˚C and 500˚C, corresponding to the dehydroxylation of $Ca(OH)_2$, was used to determine its residual content according to Equation (4).

$$m_{Ca(OH)_2,\ residual} = 100 \times \frac{\Delta m_{H_2O} / 18.02}{m_{950} / 74.09} \tag{4}$$

Finally, the amount of $Ca(OH)_2$ consumed by the pozzolanic reaction was cal-

culated as indicated in Equation (5) and expressed as grams of $Ca(OH)_2$ per 100 g of SCM (g/100g SCM).

$$m_{Ca(OH)_{2,\ consumption}} = 100 \times \frac{m_{0,\ Ca(OH)_2} - m_{0,Ca(OH)_2,\ residual}}{m_{0,\ SCM}} \quad (5)$$

where:

Δm_{H_2O} refers to the mass loss corresponding to $Ca(OH)_2$ dehydroxylation from the TG curve.

m_{950} is the mass of the sample at 950˚C.

74.09 and 18.02 are the molecular masses of calcium hydroxide and water, respectively.

$m_{Ca(OH)_2,\ residual}$ is the amount of unconsumed calcium hydroxide in the sample after curing.

$m_{0,\ Ca(OH)_2}$ is the initial mass of calcium hydroxide in the R3 paste mixture.

$m_{0,\ SCM}$ is the initial mass of SCM.

3. Results and Discussions

3.1. Visual Examination of Raw and Calcined Clays

Figure 1 shows the visual appearance of both raw and calcined clays. Significant color changes were observed after calcination, suggesting possible chemical and structural transformations occurring during the process. However, for the calcined clays, the color remained unchanged over the entire calcination temperature range. Therefore, only one sample is illustrated in the figure as a representative of the calcined clays for each clay type.

Figure 1. Illustration of clay samples: (a) raw clay A; (b) ground clay A; (c) calcined clay A; (d) raw clay B; (e) ground clay B; (f) calcined clay B.

3.2. XRF Results

The chemical composition of the two clays, determined by XRF, is presented in Table 1. The primary oxides identified are silica (SiO_2), alumina (Al_2O_3), and iron oxide (Fe_2O_3). Clay A contains both a significant proportion of silica (54.10%) and alumina (39.23%), while clay B is predominantly rich in silica (71.80%) with a lower alumina content (16.90%). These results suggest that both clays are predominantly aluminosilicate-based materials with minor contents of other oxides such

as Fe_2O_3, CaO, K_2O, and TiO_2. In addition, the SiO_2/Al_2O_3 ratio provides valuable insights into the potential mineralogical composition of these clays. In fact, the SiO_2/Al_2O_3 ratio of 1.38 for clay A, typical of the 1:1 SiO_2-Al_2O_3 structure of kaolinite, suggests its potential presence in this clay. On the other hand, clay B exhibits a higher SiO_2/Al_2O_3 ratio of 4.25, suggesting the prevalence of silicate phases such as quartz or other aluminosilicate phases.

Concerning the suitability of these clays as SCMs, their chemical composition was evaluated based on the ASTM C618 requirements [33], which define the criteria for pozzolanic materials. As shown in **Table 2**, the sum of the oxides' amounts (%) (SiO_2 + Al_2O_3 + Fe_2O_3) in both clays exceeds the minimum requirement of 70%, with clay A achieving 97.56% and clay B 91.50%. This conformity to the chemical composition requirement of ASTM C618 for class N pozzolan highlights their chemical suitability as SCMs. Additionally, both clays meet the standard limits for moisture content (≤3%), with values of 1.25% and 1.26% for clay A and clay B, respectively. However, the loss on ignition (LOI) of clay A, at 15.16%, exceeds the limit of 10%, likely due to the presence of organic matter in the raw clays, which should undergo decomposition during the calcination process to obtain calcined clays normally intended for use in cementitious systems. Similar values have been reported for raw kaolinitic clays [34]-[36], while lower values were observed for calcined samples [29] [37], reflecting the effect of calcination in reducing this property.

To further illustrate the suitability of the studied clays as SCMs, their position on the CaO-SiO_2-Al_2O_3 ternary diagram (**Figure 2**) provides a visual confirmation of their pozzolanic potential. Both clays are located within the pozzolanic region, as established by Pontikes and Snellings [38]. Clay A, especially, is situated within the metakaolin domain of the diagram, further confirming the earlier suggestion of kaolinite's predominant presence in this clay.

Table 1. The chemical composition of the raw clays was measured by XRF.

	Oxides composition (%)								
Raw clays	SiO_2	Al_2O_3	Fe_2O_3	CaO	MgO	Na_2O	K_2O	TiO_2	P_2O_5
A	54.10	39.23	4.23	0.15	0	0	0.16	1.74	0.12
B	71.80	16.9	2.80	0.16	1.33	1.27	4.63	0.80	0

Table 2. Chemical requirements.

Composition (%)	ASTM C618 requirements	Clay A	Clay B
SiO_2 + Al_2O_3 + Fe_2O_3	≥70	97.56	91.5
Sulfur trioxide (SO_3)	≤4	0	0
Loss on ignition at 1000˚C (LOI)	≤10	15.16	6.63
Moisture content at 105˚C	≤3	1.25	1.26

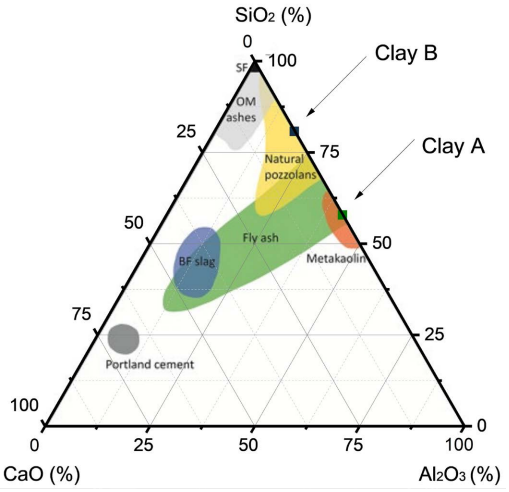

Figure 2. CaO-SiO_2-Al_2O_3 (%) ternary diagram showing clay A and clay B, respectively, in the metakaolin and natural pozzolan domains, as proposed by Pontikes and Snellings [38]. For graphical representation, oxide mass fractions were normalised to 100 before plotting.

3.3. XRD Results

As intended, the XRD analysis allowed identification of the crystalline phases present in the clays and facilitated tracking their transformation upon calcination. The diffraction patterns of both raw and calcined clays are presented in **Figure 3**. A detailed examination of these patterns reveals key differences in the mineralogical composition of the two clays.

Clay A is predominantly composed of kaolinite (K), along with anatase (A) and hematite (H). In contrast, clay B is mainly composed of quartz (Q), muscovite (M), and a minor amount of kaolinite (K). These findings are consistent with the chemical composition obtained from XRF analysis. The previous findings from this analysis are confirmed by the abundant presence of kaolinite in clay A, while the presence of anatase and hematite is validated by the significant proportions of TiO_2 and Fe_2O_3 previously identified in this clay. For clay B, the dominance of quartz is confirmed by the high SiO_2 content, while its prominent K_2O content among the secondary oxides supports the presence of muscovite in the clay.

The card numbers of the powder diffraction files (PDF) corresponding to the identified minerals are provided in **Table 3** and have also been referenced in other studies.

Table 3. Crystalline phases with their corresponding chemical formulas and PDF numbers.

Mineral name	Chemical formula	PDF number	Supporting References
Kaolinite	$Al_2Si_2O_5(OH)_4$	96-900-9231	[39]-[41]
Anatase	TiO_2	96-901-5930	[42]
Hematite	Fe_2O_3	96-900-0140	[43]
Quartz	SiO_2	96-901-3322	[40] [44]
Muscovite	$KAl_2(AlSi_3O_{10})(OH)_2$	96-900-5188	[45]

As shown by the diffraction patterns of clay A (**Figure 3(a)**), the most significant peaks of kaolinite (K) appear at $2\theta = 12.3^\circ$, 19.83°, 24.86°, 38.45°, 45.55°, and 62.24°. For clay B (**Figure 3(b)**), the few reflections associated with kaolinite are observed at similar positions at $2\theta = 12.33^\circ$ and 19.70°. These peak positions align with those reported by [46]-[50], who also identified kaolinite at the same, or approximately the same, diffraction angles, confirming the reliability of these findings.

Comparing these results with those of Anove *et al.* [20], who previously investigated clay samples obtained from the same quarries, both studies found kaolinite as the major mineral in clay A and as a minor component in clay B. However, the present study also detected hematite in clay A, which was not observed in the earlier study. This presence of hematite, a well-known iron oxide (Fe_2O_3), may explain the slight reddish-brown colour observed in the calcined clay (**Figure 1(c)**). In fact, the ambient environment in the furnace during calcination may contribute to further oxidation of this mineral. This phenomenon aligns with a previous study by Martirena Hernàndez *et al.* [51], where XRD analysis confirmed the presence of hematite in red calcined clays obtained in an oxygen-available environment, contributing to their reddish hue, while black calcined clays showed traces of magnetite (Fe_3O_4) under atmospheric control conditions. Similarly, the reddish color observed in the calcined clay A in this study could be attributed to the presence of hematite, confirming the influence of this mineral on the coloration of calcined clays. For clay B, while both studies found quartz as the dominant component, the earlier study by Anove and co-workers [20] reported illite instead of muscovite, which is identified in the present study. These differences could be attributed to various factors such as geological variations, sample processing, and the employed methods, particularly the databases used for mineral identification. In fact, the previous study used the COD database, while the current study relied on both COD and ICDD powder diffraction files (PDF-2) databases. This variation in databases could contribute to differences in mineral identification, as they may provide different details and precision in XRD data. Additionally, similar diffraction peaks are often attributed to both minerals in the literature [52]-[55].

Regarding the crystallinity of the clays, clay A exhibits a predominance of the kaolinite phase, which contributes to its overall crystallinity. However, the presence of less intense and broader peaks suggests that portions of the structure may be poorly crystallized. In contrast, clay B demonstrates higher crystallinity, as indicated by the sharper and more defined peaks associated with quartz and muscovite.

The calcination process at different temperatures ranging from 700˚C to 900˚C led to noticeable changes in the mineralogical composition of both clays, particularly in the kaolinite phases (**Figure 4**). As calcination progresses, there is a notable reduction in the intensity of the kaolinite peaks, whereas the intensity of anatase and hematite in clay A, and muscovite and quartz in clay B, remains relatively unchanged.

These observations suggest that while kaolinite ($Al_2Si_2O_5(OH)_4$) undergoes a significant transformation into metakaolinite ($2SiO_2Al_2O_3$), an amorphous and more reactive phase, the other minerals in the clays are largely unaffected and do not undergo significant structural changes within the studied temperature range. This transformation of kaolinite has important implications for the overall reactivity of the clays in cementitious systems. The formation of amorphous metakaolinite is critical for enhancing their pozzolanic reactivity, as its reactive sites, produced by heat treatment, enable effective interaction commonly leading to the formation of additional cementitious compounds, such as calcium silicate hydrates (C-S-H) and calcium aluminate hydrates (C-A-H), which contribute to the overall strength and durability of the cementitious material [3]. This being so, the more amorphous structure obtained for clay A after calcination could make it a more reactive pozzolan, potentially enhancing its suitability for use as supplementary cementitious material (SCM). However, the presence of stable and unreactive phases like quartz and muscovite in clay B may not directly influence the pozzolanic reactivity of the clays but could have other effects, either favourable or damaging, on the overall performance of cement.

Turning to the effects of varying calcination temperatures, it is observable for both clays that increasing the calcination temperature above 700˚C does not produce significant changes in the diffraction patterns. The structural transformations induced by the calcination process remained similar as the temperature increased. This finding aligns with the stability of the color observed in the calcined clays within the calcination temperature range and could suggest that calcination at 700˚C for 2 h may be sufficient to induce the desired phase transformation in the clays.

Additionally, it has been shown that calcination between 700˚C and 900˚C effectively induces the formation of a reactive amorphous metakaolin phase, which is essential to enhance the pozzolanic properties of kaolinitic clays. However, beyond 900˚C, the risk of over-calcination increases [56] and may lead to the development of more stable and non-reactive phases, which reduce the overall reactivity [57] [58].

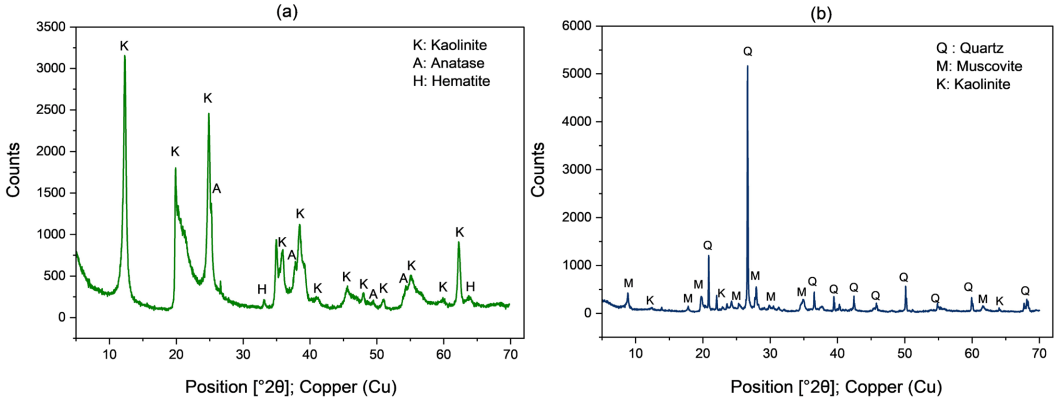

Figure 3. XRD patterns of raw materials: (a) clay A and (b) clay B.

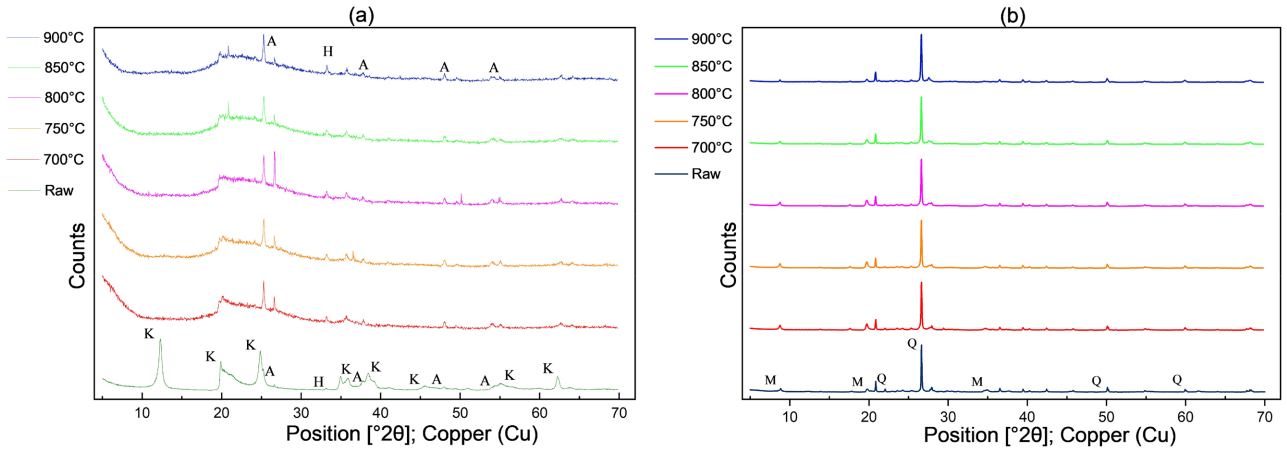

Figure 4. XRD patterns of (a) raw and calcined clay A; (b) raw and calcined clay B.

3.4. FTIR Results

To further investigate the structural and chemical characteristics of the clays, FTIR analysis was also conducted to examine the functional groups present in the raw clay samples and to evaluate the chemical changes induced by the calcination process.

The FTIR spectra of the raw clays (**Figure 5**) display distinct absorption bands that align with the mineral phases identified by XRD analysis. In clay A, kaolinite exhibited three absorption bands in the OH stretching region at 3690, 3648, and 3620 cm^{-1}, characteristic of its structure [59]-[61]. Three additional bands, also typical of the kaolinite structure, were observed in the range of Si-O stretching vibrations at 1115, 1025, and 995 cm^{-1} [62]. The absorption band at 909 cm^{-1} is related to the Al-OH deformation within the octahedral layer of kaolinite, while the bands at 526 cm^{-1} and 452 cm^{-1} correspond, respectively, to the Si-O-Al and Si-O-Si deformations [60], further confirming the presence of kaolinite in this clay. Additionally, the band at 526 cm^{-1} could also be associated with the presence of hematite [63], while the one at 640 cm^{-1} is often assigned to Si-O vibrations in quartz or kaolinite [60]. Furthermore, the doublet at 746 and 790 cm^{-1} is typically attributed to the symmetric stretching vibration of Si-O-Si bonds in quartz [64] or Si-O-Al vibrations in kaolinite [65]. However, as quartz was not identified in this clay, these vibration bands are more likely attributable to kaolinite. Concerning the band at 526 cm^{-1}, which could correspond either to kaolinite or hematite, further examination of the FTIR spectra of the calcined clays could help confirm its origin, as the decomposition of kaolinite during calcination would alter its characteristic bands, while that of hematite would remain unchanged or only slightly modified. Clay B, on the other hand, shows distinct absorption bands that could initially be associated with its three mineral phases identified by the XRD analysis. The bands at 3628 and 909 cm^{-1}, corresponding respectively to the stretching vibration of OH groups and the deformation of Al-OH and Si-O-Al groups, are characteristic of both muscovite and kaolinite. Their low intensity reflects the fact

that these two minerals were identified as secondary phases. The other bands at 998, 694, 648, 516, and 457 cm^{-1}, indicative of Si-O, Si-O-Si, and Si-O-Al vibrations, suggest the presence of silicate and aluminosilicate structures that could correspond to quartz, muscovite, and kaolinite. However, since quartz was identified as the dominant mineral in this clay, it is probable that these bands correspond to quartz. For this clay also, an examination of the FTIR spectra of the calcined clays would be necessary to confirm this, as the stability of quartz over the calcination temperature range would not induce any alteration of these bands. The same suggestions are applicable to the doublet at 796 and 778 cm^{-1}.

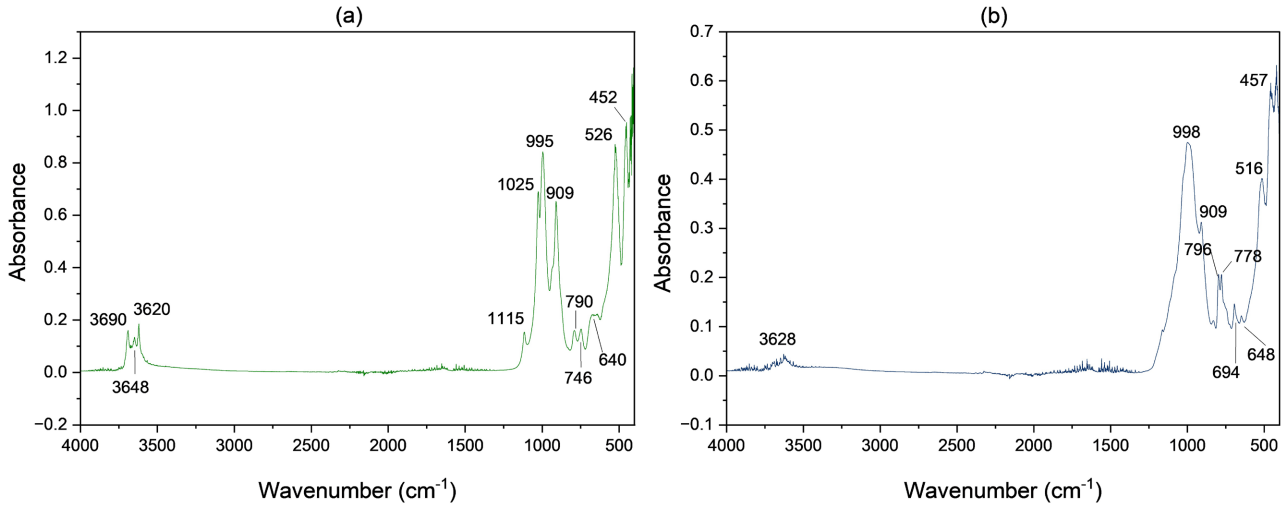

Figure 5. FTIR absorbance spectra of raw materials: (a) clay A and (b) clay B.

Regarding the effects of calcination, the FTIR spectra of calcined clays (**Figure 6**) reveal significant modifications in the absorption bands compared to the raw clays, particularly for clay A. For this clay, the characteristic OH stretching bands of kaolinite at 3690, 3648, and 3620 cm^{-1}, as well as the Al-OH deformation band at 909 cm^{-1}, completely disappeared upon calcination, indicating the dehydroxylation of kaolinite. Similarly, the absence of the bands at 1115 and 1025 cm^{-1}, associated with Si-O stretching vibrations, indicates the destruction of the kaolinite framework. Additionally, the band initially observed at 995 cm^{-1} shifted to a broader band, suggesting the formation of a new silicate structure, likely amorphous silica. Moreover, the absence of the 526 cm^{-1} band supports the earlier suggestion that this band originates from kaolinite, as hematite would not completely disappear under the applied calcination conditions. Furthermore, the doublet at 746 and 790 cm^{-1}, previously attributed to Si-O-Si of quartz or Si-O-Al vibrations in kaolinite, shifted to a single broad peak, reflecting a structural reorganization linked to kaolinite. These observations confirm that the transformations in clay A are mainly due to the decomposition of kaolinite, which is in agreement with the findings of [62] and [66], where similar modifications were observed for kaolinitic clays. For clay B, fewer transformations were observed. The disappearance of the

OH stretching band at 3628 cm^{-1} and the Al-OH deformation band at 909 cm^{-1} indicates the loss of hydroxyl groups of kaolinite or muscovite. However, the persistence of the other bands, including the doublet at 796 and 778 cm^{-1}, across the calcination temperature range suggests that these vibrations are associated with quartz, the dominant mineral in this clay.

Moreover, as revealed by the XRD results and the color examination, for both clays, changing the calcination temperature did not lead to significant variations in the FTIR spectra of the calcined clays, supporting the suggestion that a calcination temperature of 700˚C would be sufficient to achieve reactive metakaolin.

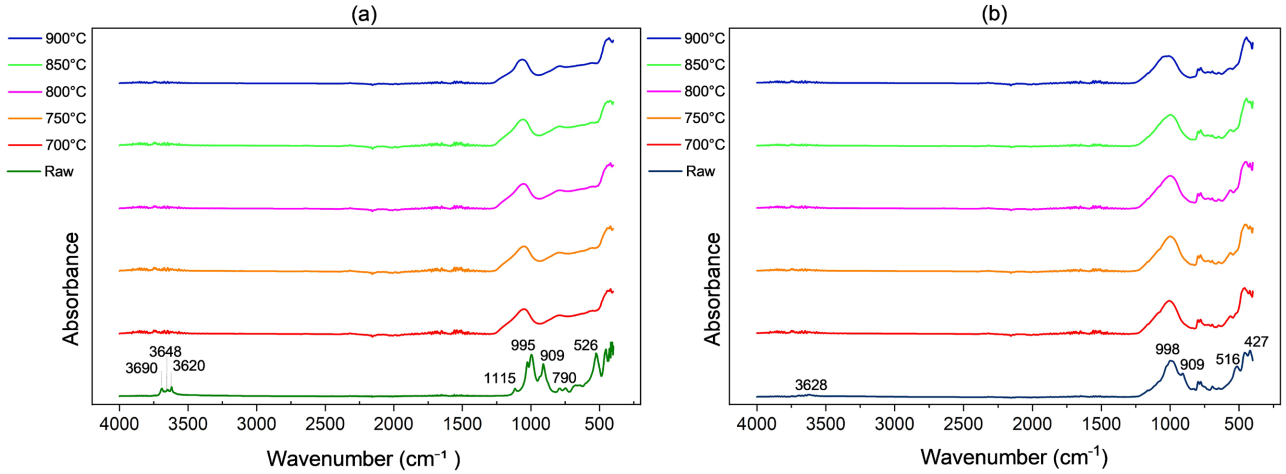

Figure 6. FTIR spectra of (a) raw and calcined clay A and (b) raw and calcined clay B.

3.5. TGA Results

The thermogravimetric (TG) and derivative thermogravimetric (DTG) curves shown in **Figure 7** and **Figure 8** illustrate the thermal behavior of the clays.

For both clays, two major mass loss stages were observed. The first stage, occurring below 200˚C, corresponds to the release of physically absorbed water, which is typical for clay minerals. For clay A, the second stage, occurring between 400˚C and 600˚C, is attributed to the dehydroxylation of kaolinite, leading to the formation of metakaolin. The quantification of this dehydroxylation process from the TG curve revealed a mass loss of 11.42% ± 0.13%, which is close to the theoretical value of 13.95% commonly reported for pure kaolinite [67] [68]. This experimental TG mass loss corresponds to a calculated kaolinite content of 81.80% ± 0.94%, confirming the predominance of kaolinite in its composition. The DTG curve, showing a characteristic peak at 524.9˚C, provides additional information on the dehydroxylation of kaolinite in this clay. This peak value is also close to that reported for similar kaolinite content in clay samples.

For clay B, the mass loss observed during the second phase continues beyond 600˚C, suggesting that the overall loss could be associated with the decomposition of hydroxyl groups from both kaolinite and muscovite. However, the quantification of TG mass loss within the kaolinite decomposition range was found to be

2.58% ± 0.08%. This corresponds to a calculated kaolinite content of 18.53% ± 0.61%. These values, significantly lower than those obtained for clay A, go with the minor presence of kaolinite observed in this clay through XRD and FTIR analyses. On the DTG curve of this clay (**Figure 8(b)**), two peaks were observed between 400˚C and 600˚C. While the peak at 571.5˚C is likely attributable to kaolinite transformation into metakaolinite, the more intense one at 478.9˚C may reflect an early-stage dehydroxylation of muscovite. This suggestion is supported by the previous analyses, which indicate a greater presence of muscovite than kaolinite in this clay. Moreover, muscovite is known to undergo complete dehydroxylation between 700˚C and 900˚C [69] [70]. However, no characteristic DTG peak was observed in this temperature range, despite its confirmed presence by XRD analysis. This absence of thermal signal, combined with the presence of two DTG peaks within the kaolinite transformation range, suggests that muscovite may have begun dehydroxylation earlier than expected or may have undergone partial dehydroxylation, overlapping with kaolinite. Such interference could contribute to an overestimation of the kaolinite content, as the method used relies on the mass loss between 400˚C and 600˚C. This phenomenon has been reported by Mañosa *et al.* [71] and Alujas *et al.* [28] for clays containing kaolinite and other mineral phases like muscovite, illite, and montmorillonite. Alujas *et al.* [28] have also mentioned this phenomenon as one of the main factors affecting the accuracy of this estimation method. These findings highlight the complexity of the thermal behaviour of clay B and emphasize the need, in such cases, to use complementary techniques such as Rietveld refinement of XRD data to confirm the estimated content of each phase.

For calcined clays, TGA analysis was conducted to assess the calcination efficiency by quantifying their remaining kaolinite content after calcination (**Figure 9**). In fact, a significant residual mass loss between 400˚C - 600˚C would suggest incomplete dehydroxylation of kaolinite, thereby indicating insufficient calcination. For clay A, the results show nearly complete dehydroxylation of kaolinite, with a decrease in its residual content as calcination temperature increases. At 700˚C, only 3.72% ± 0.12% of kaolinite remains, indicating that most of the kaolinite has undergone dehydroxylation, with 78.08% ± 0.18% reacted during calcination. Between 750˚C and 900˚C, the residual kaolinite content varies from 1.61% ± 0.10% to 1.47% ± 0.13%, with the calcined kaolinite content stabilizing around 80%, suggesting that calcination is nearly completed at 750˚C. The slight fluctuation observed at 800˚C could be due to experimental uncertainty. For clay B, two distinct phases of transformation were observed. The first occurs between 700˚C and 750˚C, where the residual kaolinite content initially reaches 1.47% ± 0.04% at 700˚C but then increases to 5.80% ± 0.03% at 750˚C. The second stage occurs between 800˚C and 900˚C, with a gradual decrease in the residual kaolinite content from 4.69% ± 0.01% at 800˚C to 0.43% ± 0.02% at 900˚C. This unexpected observation supports the earlier suggestion of a possible overlap of the dehydroxylation signals of kaolinite and muscovite, both present in this clay. This could

explain its less predictable thermal evolution.

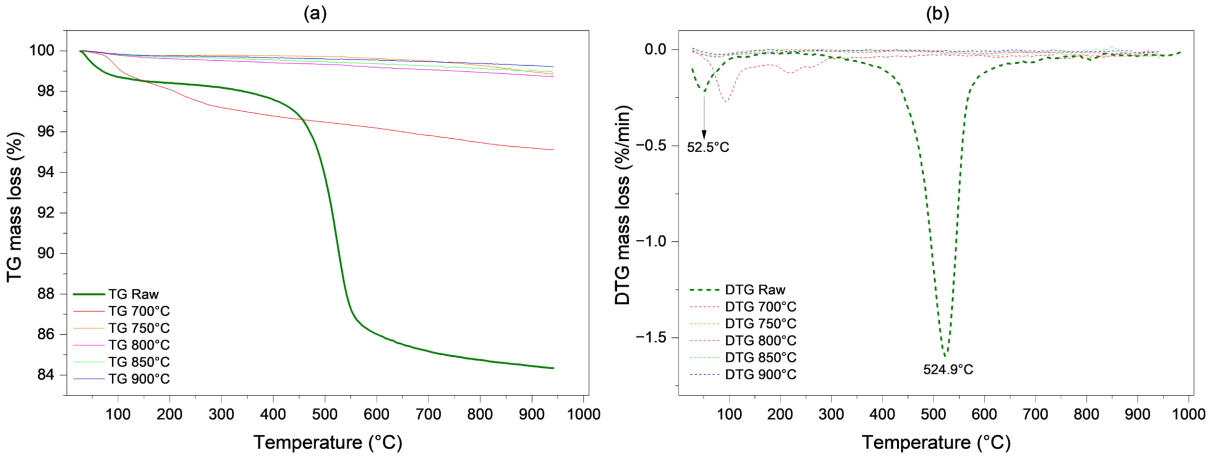

Figure 7. TG curves of raw and calcined clay A (a) and DTG curves of raw and calcined clay A (b).

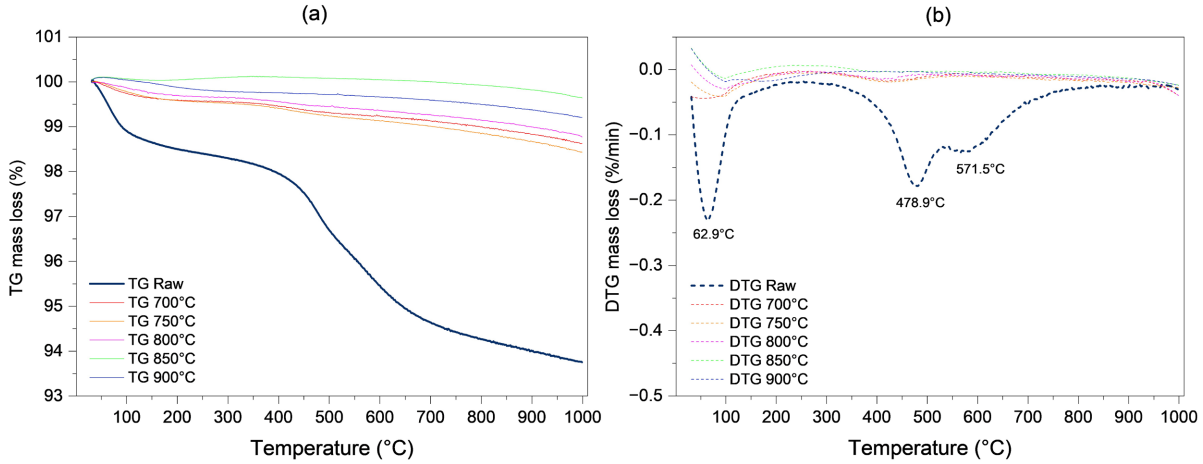

Figure 8. TG curves of raw and calcined clay B (a) and DTG curves of raw and calcined clay B (b).

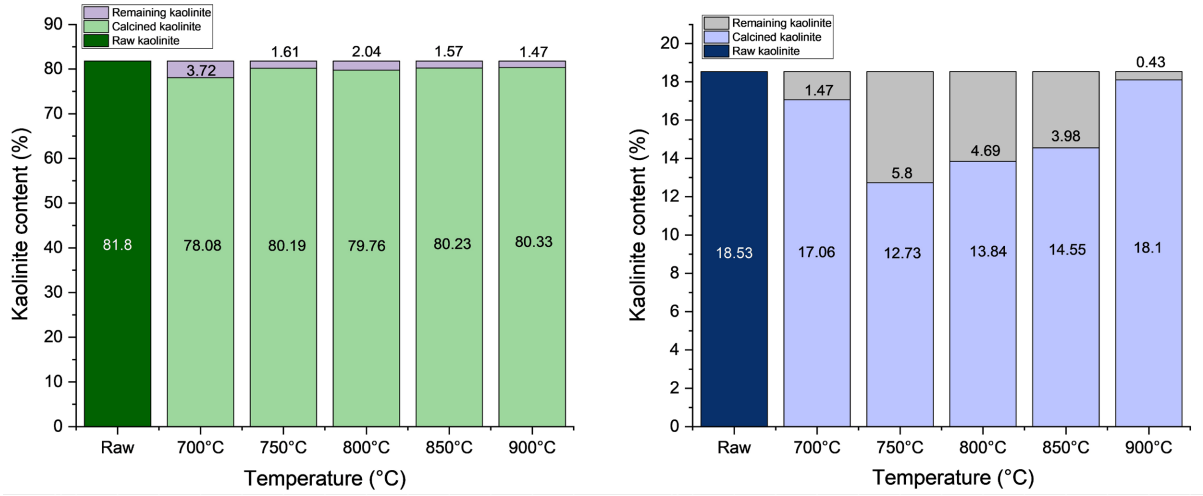

Figure 9. Kaolinite content evolution during calcination, measured from TGA analysis: (a) clay A and (b) clay B.

Overall, the TGA analysis revealed ongoing thermal modifications across the entire calcination temperature range for both clays, a fact that was less observable in XRD and FTIR results. In fact, while these two previous analyses suggested that calcination at 700˚ was sufficient, TGA provides more precise information, indicating that slight thermal transformations continue beyond this temperature. For clay A, the rate of kaolinite transformation becomes less significant beyond 750˚C, making it an ideal temperature for calcination. For clay B, its thermal complexity makes the determination of an optimal calcination temperature more challenging.

3.6. Results of the R3 Test

To further evaluate the reactivity of the clays, a TGA-based R3 test was performed to quantify their calcium hydroxide consumption. In cementitious systems, pozzolanic materials have the ability to react with calcium hydroxide to form additional hydrated compounds that enhance the mechanical properties and the durability of the cement matrix [72]. The amount of $Ca(OH)_2$ consumed by a material during the R3 test is therefore an indicator of its pozzolanic reactivity. The more calcium hydroxide it consumes, the more reactive it is considered. According to the literature, a material is considered pozzolanic if its $Ca(OH)_2$ consumption is at least 660 mg per gram of pozzolan [73]-[75], which corresponds to 66 g per 100 g of pozzolan. The results are summarised in **Table 4**, and values are expressed as mean ± standard deviation.

In their raw state, the two clays showed relatively low $Ca(OH)_2$ consumption. However, even before thermal activation, both exceeded the minimum value of 66 g/100g, which is indicative of good pozzolanic reactivity. Raw clay A consumed (76.17 ± 6.46) g/100g, while raw clay B consumed (111.07 ± 14.90) g/100g.

Upon calcination, a significant improvement in reactivity was observed, particularly for clay A. At 700˚C, its $Ca(OH)_2$ consumption increased to (202.44 ± 2.64) g/100g, nearly three times higher than that of the raw clay. However, increasing the calcination temperature up to 900˚C did not significantly affect the reactivity, as the $Ca(OH)_2$ consumption varied between (202.44 ± 2.64) and (205.72 ± 3.60) g/100g (**Table 4**). This relatively constant value indicates that the clay achieved almost maximum pozzolanic reactivity around 700˚C - 750˚C. This aligns with the previous analyses, which showed a nearly complete transformation of kaolinite over the same temperature range. Calcination also improved the reactivity of clay B, but less significantly than for clay A. With increasing temperature, the $Ca(OH)_2$ consumption gradually increased from (129.05 ± 20.25) g/100g at 700˚C to (153.60 ± 14.27) g/100g at 900˚C. Unlike clay A, clay B showed no constancy in its reactivity. Its continuous increase up to 900˚C is consistent with the gradual dehydroxylation signals observed in TGA analysis. Clay B reached its maximum pozzolanic reactivity at 900˚C. However, even at this temperature, its $Ca(OH)_2$ consumption remained significantly lower than that of clay A.

The lower reactivity of clay B compared to clay A can be explained by its lower kaolinite content with a higher proportion of quartz, a non-reactive phase. A part

of its reactivity during calcination could come from the possible transformation of muscovite, which is less reactive than metakaolinite [71]. This explains why its reactivity improved slowly without reaching that of clay A, even though, in their raw state, it showed the best reactivity.

In summary, the R3 test confirmed that both clays are reactive, especially after calcination. Clay A reached a level of reactivity far above the 66 g/100g minimum required for pozzolanic materials. It therefore appears to be a promising pozzolanic material. Clay B, although less reactive than clay A, also showed significant reactivity after calcination. These results confirm the potential of the two clays to be used as SCMs in blended cement.

Table 4. Calcium hydroxide consumption of raw and calcined clays A and B, based on the R3 test.

	Samples	
Temperatures	Clay A (g $Ca(OH)_2$/100 g SCM)	Clay B (g $Ca(OH)_2$/100 g SCM)
Raw	76.17 ± 6.46	111.07 ± 14.90
700˚C	202.44 ± 2.64	129.05 ± 20.25
750˚C	204.06 ± 4.40	138.68 ± 4.88
800˚C	203.32 ± 4.95	145.08 ± 3.86
850˚C	204.34 ± 4.34	151.57 ± 1.21
900˚C	205.72 ± 3.60	153.60 ± 14.27

4. Conclusions

This work investigated the characterisation and the pozzolanic reactivity of two Togolese clays to assess their potential as SCMs. Through a series of instrumental techniques, including XRF, XRD, FTIR, and TGA, the physicochemical properties of the clays were examined. The findings revealed that clay A is predominantly composed of kaolinite, making it suitable for calcination into metakaolinite, a highly reactive pozzolanic phase in clays.

The clays subjected to different calcination temperatures ranging from 700˚C to 900˚C showed significant transformations, particularly clay A, in which kaolinite was effectively converted into metakaolinite. For this clay, while XRD and FTIR analyses suggested that calcination at 700˚C for 2 h is sufficient to achieve the desired phase transformation in both clays, TGA results indicated that, for clay A, 750˚C might be more optimal. In contrast, clay B, which is rich in quartz with a minor amount of kaolinite, exhibited complex thermal behavior, making its optimal calcination temperature less predictable. Despite these differences, both clays met the ASTM C618 chemical requirements for pozzolanic materials, with the combined content of SiO_2, Al_2O_3, and Fe_2O_3 exceeding 70%.

Moreover, the pozzolanic reactivity assessed through the TGA-based R3 test further confirmed the effectiveness of both clays as SCMs, with clay A exhibiting notably higher reactivity compared to clay B. However, further studies could also

focus on evaluating the performance of these clays in cement mixtures to fully investigate their potential in sustainable construction applications.

Funding

This work was financially supported by the "Service de Coopération et d'Action Culturelle (SCAC)" of the French Embassy in Togo.

Acknowledgements

The authors would like to thank M. Ruben Vera from the Henri Longchamp Diffractometry Center at Claude Bernard University Lyon-1 for the XRD analyses, as well as the technical staff of LAGEPP for their support.

Conflicts of Interest

The authors declare no conflicts of interest regarding the publication of this paper.

References

[1] Supriya, Chaudhury, R., Sharma, U., Thapliyal, P.C. and Singh, L.P. (2023) Low-CO_2 Emission Strategies to Achieve Net Zero Target in Cement Sector. *Journal of Cleaner Production*, **417**, Article ID: 137466. https://doi.org/10.1016/j.jclepro.2023.137466

[2] Snellings, R., Mertens, G. and Elsen, J. (2012) Supplementary Cementitious Materials. *Reviews in Mineralogy and Geochemistry*, **74**, 211-278. https://doi.org/10.2138/rmg.2012.74.6

[3] Weise, K., Endell, L.M., Ukrainczyk, N. and Koenders, E. (2024) Pozzolanic Metakaolin Reactivity: Time-Dependent Influence of Calcium Hydroxide, Alkali Hydroxides, and Sulfates. *Construction and Building Materials*, **431**, Article ID: 136534. https://doi.org/10.1016/j.conbuildmat.2024.136534

[4] Scrivener, K., Martirena, F., Bishnoi, S. and Maity, S. (2018) Calcined Clay Limestone Cements (LC^3). *Cement and Concrete Research*, **114**, 49-56. https://doi.org/10.1016/j.cemconres.2017.08.017

[5] Antoni, M., Rossen, J., Martirena, F. and Scrivener, K. (2012) Cement Substitution by a Combination of Metakaolin and Limestone. *Cement and Concrete Research*, **42**, 1579-1589. https://doi.org/10.1016/j.cemconres.2012.09.006

[6] Martirena, F. and Scrivener, K. (2017) Low Carbon Cement LC^3 in Cuba: Ways to Achieve a Sustainable Growth of Cement Production in Emerging Economies. In: Martirena, F., Favier, A. and Scrivener, K., Eds., *Calcined Clays for Sustainable Concrete*, Springer, 318-321. https://doi.org/10.1007/978-94-024-1207-9_51

[7] Hernandez, J.F.M. and Scrivener, K. (2015) Development and Introduction of a Low Clinker, Low Carbon, Ternary Blend Cement in Cuba. In: Scrivener, K. and Favier, A., Eds., *Calcined Clays for Sustainable Concrete*, Springer, 323-329. https://doi.org/10.1007/978-94-017-9939-3_40

[8] (2025) History LC3-Project—LC3. https://lc3.ch/history-of-lc3-research/

[9] Scrivener, K.L. (2014) Options for the Future of Cement. *Indian Concrete Journal*, **88**, 11-21.

[10] Bishnoi, S., Maity, S., Mallik, A., Joseph, S. and Krishnan, S. (2014) Pilot Scale Manufacture of Limestone Calcined Clay Cement: The Indian Experience. *Indian Concrete Journal*, **88**, 22-28.

[11] Mañosa, J., Calderón, A., Salgado-Pizarro, R., Maldonado-Alameda, A. and Chimenos, J.M. (2024) Research Evolution of Limestone Calcined Clay Cement (LC^3), a Promising Low-Carbon Binder—A Comprehensive Overview. *Heliyon*, **10**, e25117. https://doi.org/10.1016/j.heliyon.2024.e25117

[12] Kafodya, I., Basuroy, D., Marangu, J.M., Kululanga, G., Maddalena, R. and Novelli, V.I. (2023) Mechanical Performance and Physico-Chemical Properties of Limestone Calcined Clay Cement (LC3) in Malawi. *Buildings*, **13**, Article 740. https://doi.org/10.3390/buildings13030740

[13] Marangu, J.M. (2020) Physico-Chemical Properties of Kenyan Made Calcined Clay - Limestone Cement (LC3). *Case Studies in Construction Materials*, **12**, e00333. https://doi.org/10.1016/j.cscm.2020.e00333

[14] Babafemi, A.J., Knobel, H., Kolawole, J.T., Oyebanjo, O.M., Bukalo, N.N., Paul, S.C., *et al.* (2022) Performance of Selected South African Kaolinitic Clays for Limestone Calcined Clay Cement. *Applied Sciences*, **12**, Article 10751. https://doi.org/10.3390/app122110751

[15] Akindahunsi, A.A., Avet, F. and Scrivener, K. (2020) The Influence of Some Calcined Clays from Nigeria as Clinker Substitute in Cementitious Systems. *Case Studies in Construction Materials*, **13**, e00443. https://doi.org/10.1016/j.cscm.2020.e00443

[16] Bediako, M., Purohir, S.S. and Kevern, J.T. (2017) An Investigation into Ghanaian Calcined Clay as a Supplementary Cementitious Material. *ACI Materials Journal*, **114**, 889-896. https://doi.org/10.14359/51700896

[17] Ramadji, C., Messan, A., Sore, S.O., Prud'homme, E. and Nshimiyimana, P. (2022) Microstructural Analysis of the Reactivity Parameters of Calcined Clays. *Sustainability*, **14**, Article 2308. https://doi.org/10.3390/su14042308

[18] (2024) Normes de fabrication du ciment: un cadre pour garantir qualité et sécurité. République Togolaise. https://www.republicoftogo.com/toutes-les-rubriques/societe/normes-de-fabrication-du-ciment-un-cadre-pour-garantir-qualite-et-securite

[19] Pinheiro, V.D., Alexandre, J., Xavier, G.d.C., Marvila, M.T., Monteiro, S.N. and de Azevedo, A.R.G. (2023) Methods for Evaluating Pozzolanic Reactivity in Calcined Clays: A Review. *Materials*, **16**, Article 4778. https://doi.org/10.3390/ma16134778

[20] Anove, K.M., Tchegueni, S., Degbe, K.A., Fiaty, K., Koriko, M., Drogui, P., *et al.* (2022) Physico-Chemical and Mineralogical Characterizations of Two Togolese Clays for Geopolymer Synthesis. *Journal of Minerals and Materials Characterization and Engineering*, **10**, 400-409. https://doi.org/10.4236/jmmce.2022.105028

[21] Overmann, S., Vollpracht, A. and Matschei, T. (2024) Reactivity of Calcined Clays as SCM—A Review. *Materials*, **17**, Article 312. https://doi.org/10.3390/ma17020312

[22] Overmann, S., Eggimann, M., Vollpracht, A. and Matschei, T. (2024) Impact of Clay Reactivity on the Hydration of Calcined Clay Limestone Cements. *Construction and Building Materials*, **449**, Article ID: 138455. https://doi.org/10.1016/j.conbuildmat.2024.138455

[23] Şahin, F., Uysal, M. and Canpolat, O. (2021) Systematic Evaluation of the Aggregate Types and Properties on Metakaolin Based Geopolymer Composites. *Construction and Building Materials*, **278**, Article ID: 122414. https://doi.org/10.1016/j.conbuildmat.2021.122414

[24] Qian, X., Li, M., Wang, J., Wang, L., Chen, P., Fang, Y., *et al.* (2022) A Bio-Inspired, Plant-Derived Admixture for Metakaolin Blended Cement Mortars. *Construction and Building Materials*, **354**, Article ID: 129185. https://doi.org/10.1016/j.conbuildmat.2022.129185

[25] Peng, Y. and Unluer, C. (2024) Understanding the Rheological Behavior of Reactive Magnesia-Metakaolin System in the Context of Digital Construction. *Cement and Concrete Composites*, **149**, Article ID: 105534. https://doi.org/10.1016/j.cemconcomp.2024.105534

[26] Cao, Y., Wang, Y., Zhang, Z., Ma, Y. and Wang, H. (2021) Turning Sandstone Clay into Supplementary Cementitious Material: Activation and Pozzolanic Reactivity Evaluation. *Composites Part B*: *Engineering*, **223**, Article ID: 109137. https://doi.org/10.1016/j.compositesb.2021.109137

[27] Shvarzman, A., Kovler, K., Grader, G.S. and Shter, G.E. (2003) The Effect of Dehydroxylation/Amorphization Degree on Pozzolanic Activity of Kaolinite. *Cement and Concrete Research*, **33**, 405-416. https://doi.org/10.1016/s0008-8846(02)00975-4

[28] Alujas, A., Fernández, R., Quintana, R., Scrivener, K.L. and Martirena, F. (2015) Pozzolanic Reactivity of Low Grade Kaolinitic Clays: Influence of Calcination Temperature and Impact of Calcination Products on OPC Hydration. *Applied Clay Science*, **108**, 94-101. https://doi.org/10.1016/j.clay.2015.01.028

[29] Avet, F. and Scrivener, K. (2018) Investigation of the Calcined Kaolinite Content on the Hydration of Limestone Calcined Clay Cement (LC^3). *Cement and Concrete Research*, **107**, 124-135. https://doi.org/10.1016/j.cemconres.2018.02.016

[30] Scrivener, K., Snellings, R. and Lothenbach, B. (2016) A Practical Guide to Microstructural Analysis of Cementitious Materials. CRC Press.

[31] Sivakumar, P.P., Matthys, S., De Belie, N. and Gruyaert, E. (2021) Reactivity Assessment of Modified Ferro Silicate Slag by R^3 Method. *Applied Sciences*, **11**, Article 366. https://doi.org/10.3390/app11010366

[32] ASTM C1897-20 (2020) Standard Test Methods for Measuring the Reactivity of Supplementary Cementitious Materials by Isothermal Calorimetry and Bound Water Measurements. https://store.astm.org/c1897-20.html

[33] ASTM International ASTM C618-22 (2022) Standard Specification for Coal Fly Ash and Raw or Calcined Natural Pozzolan for Use in Concrete. https://doi.org/10.1520/C0618-22

[34] Mallik, A., Barik, A.K. and Pal, B. (2015) Comparative Studies on Physico-Mechanical Properties of Composite Materials of Low Density Polyethylene and Raw/Calcined Kaolin. *Journal of Asian Ceramic Societies*, **3**, 212-216. https://doi.org/10.1016/j.jascer.2015.03.001

[35] Adeleke, B., Kinuthia, J. and Oti, J. (2020) Strength and Swell Performance of High-Sulphate Kaolinite Clay Soil. *Sustainability*, **12**, Article 10164. https://doi.org/10.3390/su122310164

[36] Malacarne, C.S., Longhi, M.A., Silva, M.R.C., Gonçalves, J.P., Rodríguez, E.D. and Kirchheim, A.P. (2021) Influence of Low-Grade Materials as Clinker Substitute on the Rheological Behavior, Hydration and Mechanical Performance of Ternary Cements. *Case Studies in Construction Materials*, **15**, e00776. https://doi.org/10.1016/j.cscm.2021.e00776

[37] Avet, F., Li, X. and Scrivener, K. (2018) Determination of the Amount of Reacted Metakaolin in Calcined Clay Blends. *Cement and Concrete Research*, **106**, 40-48. https://doi.org/10.1016/j.cemconres.2018.01.009

[38] Pontikes, Y. and Snellings, R. (2014) Cementitious Binders Incorporating Residues. In: Worrell, E. and Reuter, M.A., Eds., *Handbook of Recycling*, Elsevier, 219-229. https://doi.org/10.1016/b978-0-12-396459-5.00016-7

[39] Zat, T., Bandieira, M., Sattler, N., Segadães, A.M., Cruz, R.C.D., Mohamad, G., *et al.* (2021) Potential Re-Use of Sewage Sludge as a Raw Material in the Production of Eco-

Friendly Bricks. *Journal of Environmental Management*, **297**, Article ID: 113238. https://doi.org/10.1016/j.jenvman.2021.113238

[40] El-Tanani, M., Mahasneh, B.Z., Muhana, F., El-Eswed, B., Khalili, F. and Alkhrissat, T. (2022) Blending Plastics Waste with Highly Available Jordanian Kaolin for Preparation of Alkali-Activated Mortars. *Sustainability*, **14**, Article 15742. https://doi.org/10.3390/su142315742

[41] Judicaël Geferson, O.O., Placide Desire, B.B., Serge, E.J., Odogu, A.N., Nsami, N.J. and Antoine, E. (2024) Sustainable and Cleaner Production of a Porous Geopolymer Support Based on Metakaolin and Natural Calcium Oxide. *Journal of Building Engineering*, **96**, Article ID: 110638. https://doi.org/10.1016/j.jobe.2024.110638

[42] Ye, K., Dasari, A. and Hooper, T.J.N. (2023) Structural Characterization and Fire Performance of Geopolymer-Glass Fiber Composite Panels. *Construction and Building Materials*, **400**, Article ID: 132633. https://doi.org/10.1016/j.conbuildmat.2023.132633

[43] García-Díaz, A., Delgado-Plana, P., Bueno-Rodríguez, S. and Eliche-Quesada, D. (2024) Investigation of Waste Clay Brick (Chamotte) Addition and Activator Modulus in the Properties of Alkaline Activation Cements Based on Construction and Demolition Waste. *Journal of Building Engineering*, **84**, Article ID: 108568. https://doi.org/10.1016/j.jobe.2024.108568

[44] Abiodun, Y.O., Olanrewaju, O.A., Gbenebor, O.P., Ochulor, E.F., Obasa, D.V. and Adeosun, S.O. (2022) Cutting Cement Industry CO_2 Emissions through Metakaolin Use in Construction. *Atmosphere*, **13**, Article 1494. https://doi.org/10.3390/atmos13091494

[45] Olaoluwa, D., Abdulmalik, A.E., Muraina, T.A., Girigisu, S. and Balogun, A.F. (2020) Dissolution of a Nigerian Sourced Muscovite Ore for Use as an Ingredient in Paint Production. *Journal of the Nigerian Society of Physical Sciences*, **2**, 128-133. https://doi.org/10.46481/jnsps.2020.89

[46] Fernandez, R., Martirena, F. and Scrivener, K.L. (2011) The Origin of the Pozzolanic Activity of Calcined Clay Minerals: A Comparison between Kaolinite, Illite and Montmorillonite. *Cement and Concrete Research*, **41**, 113-122. https://doi.org/10.1016/j.cemconres.2010.09.013

[47] Tironi, A., Trezza, M.A., Scian, A.N. and Irassar, E.F. (2014) Potential Use of Argentine Kaolinitic Clays as Pozzolanic Material. *Applied Clay Science*, **101**, 468-476. https://doi.org/10.1016/j.clay.2014.09.009

[48] Hollanders, S., Adriaens, R., Skibsted, J., Cizer, Ö. and Elsen, J. (2016) Pozzolanic Reactivity of Pure Calcined Clays. *Applied Clay Science*, **132**, 552-560. https://doi.org/10.1016/j.clay.2016.08.003

[49] Shokanov, A., Manakova, I., Vereshchak, M. and Migunova, A. (2024) Characterization of Kazakhstan's Clays by Mössbauer Spectroscopy and X-Ray Diffraction. *Minerals*, **14**, Article 713. https://doi.org/10.3390/min14070713

[50] Tironi, A., Trezza, M.A., Irassar, E.F. and Scian, A.N. (2012) Thermal Treatment of Kaolin: Effect on the Pozzolanic Activity. *Procedia Materials Science*, **1**, 343-350. https://doi.org/10.1016/j.mspro.2012.06.046

[51] Martirena Hernández, J.F., Almenares-Reyes, R., Zunino, F., Alujas-Diaz, A. and Scrivener, K.L. (2020) Color Control in Industrial Clay Calcination. *RILEM Technical Letters*, **5**, 1-7. https://doi.org/10.21809/rilemtechlett.2020.107

[52] Marsh, A., Heath, A., Patureau, P., Evernden, M. and Walker, P. (2018) Alkali Activation Behaviour of Un-Calcined Montmorillonite and Illite Clay Minerals. *Applied Clay Science*, **166**, 250-261. https://doi.org/10.1016/j.clay.2018.09.011

[53] Msinjili, N.S., Gluth, G.J.G., Sturm, P., Vogler, N. and Kühne, H. (2019) Comparison of Calcined Illitic Clays (Brick Clays) and Low-Grade Kaolinitic Clays as Supplementary Cementitious Materials. *Materials and Structures*, **52**, Article No. 94. https://doi.org/10.1617/s11527-019-1393-2

[54] Stefanini, L., Ansari, D., Walkley, B. and Provis, J.L. (2024) Characterisation of Calcined Waste Clays from Kaolinite Extraction in Alkali-Activated GGBFS Blends. *Materials Today Communications*, **38**, Article ID: 107777. https://doi.org/10.1016/j.mtcomm.2023.107777

[55] San Nicolas, R., Wang, T. and Rupasinghe, M. (2024) Effect of Calcined Clays from Victoria, Australia as Cement Substitution in Ternary Blended Cement Systems. *Case Studies in Construction Materials*, **20**, e02860. https://doi.org/10.1016/j.cscm.2024.e02860

[56] Zunino, F. and Scrivener, K. (2024) Reactivity of Kaolinitic Clays Calcined in the 650˚C - 1050˚C Temperature Range: Towards a Robust Assessment of Overcalcination. *Cement and Concrete Composites*, **146**, Article ID: 105380. https://doi.org/10.1016/j.cemconcomp.2023.105380

[57] Almenares, R.S., Vizcaíno, L.M., Damas, S., Mathieu, A., Alujas, A. and Martirena, F. (2017) Industrial Calcination of Kaolinitic Clays to Make Reactive Pozzolans. *Case Studies in Construction Materials*, **6**, 225-232. https://doi.org/10.1016/j.cscm.2017.03.005

[58] Cardinaud, G., Rozière, E., Martinage, O., Loukili, A., Barnes-Davin, L., Paris, M., *et al.* (2021) Calcined Clay—Limestone Cements: Hydration Processes with High and Low-Grade Kaolinite Clays. *Construction and Building Materials*, **277**, Article ID: 122271. https://doi.org/10.1016/j.conbuildmat.2021.122271

[59] Tironi, A., Trezza, M.A., Scian, A.N. and Irassar, E.F. (2012) Kaolinitic Calcined Clays: Factors Affecting Its Performance as Pozzolans. *Construction and Building Materials*, **28**, 276-281. https://doi.org/10.1016/j.conbuildmat.2011.08.064

[60] Danner, T., Norden, G. and Justnes, H. (2018) Characterisation of Calcined Raw Clays Suitable as Supplementary Cementitious Materials. *Applied Clay Science*, **162**, 391-402. https://doi.org/10.1016/j.clay.2018.06.030

[61] Hazarika, A., Huang, L. and Babaahmadi, A. (2024) Characterisation, Activation, and Reactivity of Heterogenous Natural Clays. *Materials and Structures*, **57**, Article No. 68. https://doi.org/10.1617/s11527-024-02335-9

[62] Souri, A., Kazemi-Kamyab, H., Snellings, R., Naghizadeh, R., Golestani-Fard, F. and Scrivener, K. (2015) Pozzolanic Activity of Mechanochemically and Thermally Activated Kaolins in Cement. *Cement and Concrete Research*, **77**, 47-59. https://doi.org/10.1016/j.cemconres.2015.04.017

[63] Vasić, M.V., Terzić, A., Radovanović, Ž., Radojević, Z. and Warr, L.N. (2022) Alkali-activated Geopolymerization of a Low Illitic Raw Clay and Waste Brick Mixture. An Alternative to Traditional Ceramics. *Applied Clay Science*, **218**, Article ID: 106410. https://doi.org/10.1016/j.clay.2022.106410

[64] Tan, J., Cizer, Ö., De Vlieger, J., Dan, H. and Li, J. (2022) Impacts of Milling Duration on Construction and Demolition Waste (CDW) Based Precursor and Resulting Geopolymer: Reactivity, Geopolymerization and Sustainability. *Resources, Conservation and Recycling*, **184**, Article ID: 106433. https://doi.org/10.1016/j.resconrec.2022.106433

[65] Vásquez-Torres, O.O., Cabrera-Poloche, F.D. and Tobón, J.I. (2022) Performance of Low-Grade Calcined Clays as Supplementary Cementitious Material in Relation to Their Geological Characteristics. *Clays and Clay Minerals*, **70**, 233-251. https://doi.org/10.1007/s42860-022-00184-7

[66] Zunino, F., Boehm-Courjault, E. and Scrivener, K. (2020) The Impact of Calcite Impurities in Clays Containing Kaolinite on Their Reactivity in Cement after Calcination. *Materials and Structures*, **53**, Article No. 44. https://doi.org/10.1617/s11527-020-01478-9

[67] Ptáček, P., Kubátová, D., Havlica, J., Brandštetr, J., Šoukal, F. and Opravil, T. (2010) Isothermal Kinetic Analysis of the Thermal Decomposition of Kaolinite: The Thermogravimetric Study. *Thermochimica Acta*, **501**, 24-29. https://doi.org/10.1016/j.tca.2009.12.018

[68] Elhadj, M.Y. and Perrin, F.X. (2021) Influencing Parameters of Mechanochemical Intercalation of Kaolinite with Urea. *Applied Clay Science*, **213**, Article ID: 106250. https://doi.org/10.1016/j.clay.2021.106250

[69] Snellings, R., Almenares Reyes, R., Hanein, T., Irassar, E.F., Kanavaris, F., Maier, M., *et al.* (2022) Paper of RILEM TC 282-CCL: Mineralogical Characterization Methods for Clay Resources Intended for Use as Supplementary Cementitious Material. *Materials and Structures*, **55**, Article No. 149. https://doi.org/10.1617/s11527-022-01973-1

[70] Blasi, E., Di Bella, C., Choorackal, E., Maqbool, Q., Tittarelli, F., Garufi, D., *et al.* (2024) Use of Low-Grade Kaolinite Clays in the Production of Limestone Calcined Clay Cement. *Journal of Sustainable Cement-Based Materials*, **14**, 209-221. https://doi.org/10.1080/21650373.2024.2432011

[71] Mañosa, J., Alvarez-Coscojuela, A., Marco-Gibert, J., Maldonado-Alameda, A. and Chimenos, J.M. (2024) Enhancing Reactivity in Muscovitic Clays: Mechanical Activation as a Sustainable Alternative to Thermal Activation for Cement Production. *Applied Clay Science*, **250**, Article ID: 107266. https://doi.org/10.1016/j.clay.2024.107266

[72] Becerra-Duitama, J.A. and Rojas-Avellaneda, D. (2022) Pozzolans: A Review. *Engineering and Applied Science Research*, **49**, 495-504. https://ph01.tci-thaijo.org/index.php/easr/article/view/247697

[73] Alvarez-Coscojuela, A., Mañosa, J., Formosa, J. and Chimenos, J.M. (2024) Structural Characterisation and Reactivity Measurement of Chemically Activated Kaolinite. *Journal of Building Engineering*, **87**, Article ID: 109051. https://doi.org/10.1016/j.jobe.2024.109051

[74] Yamamoto, T. (2024) Formulation Optimization and Proposal of Assessed Pozzolanic-Activity Index (API) Method for Rapid Evaluation of Pozzolanic Activity of Fly Ash. *Construction and Building Materials*, **432**, Article ID: 136394. https://doi.org/10.1016/j.conbuildmat.2024.136394

[75] Su-Cadirci, T.B., Calabria-Holley, J., Ince, C. and Ball, R.J. (2023) Freeze-Thaw Resistance of Pozzolanic Hydrated Lime Mortars. *Construction and Building Materials*, **394**, Article ID: 131993. https://doi.org/10.1016/j.conbuildmat.2023.131993